Higher-order Föppl models of steady wake flows

Bartosz Protas[a)]
Department of Mathematics and Statistics, McMaster University, Hamilton, Ontario L8S 4K1, Canada

(Received 21 June 2006; accepted 10 October 2006; published online 30 November 2006)

In this paper we construct two-dimensional steady potential flows past a circular cylinder as generalizations of the point-vortex Föppl system. For a given classical Föppl system, these higher-order systems form a two-parameter family depending on the truncation order N and the area A of the vortex region desingularizing the original Föppl solution. We characterize the higher-order equilibria analytically and numerically, and show that their modified linear stability properties make the higher-order systems useful models for a class of flow control problems. © *2006 American Institute of Physics*. [DOI: 10.1063/1.2389033]

I. INTRODUCTION

In this paper we are interested in constructing and briefly analyzing a family of higher-order Föppl systems modeling steady two-dimensional (2D) flows past a cylindrical obstacle with radius R. We will assume that the domain Ω extends to infinity where the flow is given by $U_\infty \mathbf{e}_x$, with $\mathbf{e}_x$ denoting the unit vector associated with the OX axis. The "classical" Föppl system, proposed in Ref. 1, is a potential flow consisting of two counter-rotating point vortices placed exterior to the obstacle above and below the flow centerline which, together with their images inside the cylinder, are in equilibrium with the obstacle. This system admits two one-parameter families of equilibrium solutions: one with vortices located behind the obstacle [Fig. 1(a)], and another one with vortices located directly above and below the obstacle [Fig. 1(b)]. In the case of the first equilibrium the circulation of the vortices and their position are related through simple algebraic expressions; in the case of the second equilibrium such expressions are not known in closed form. Furthermore, there also exist numerous equilibria involving a larger number of vortices.[2] In the present investigation we will primarily focus on the equilibrium solution with two vortices behind the obstacle, since it is the most relevant from the physical point of view; we will refer to it as the "Föppl equilibrium."

It is known[3] that systems of point vortices are weak solutions of the 2D Euler equations. With regard to the flows past circular cylinders, it was shown computationally by Elcrat, Fornberg, Horn, and Miller in Ref. 4 that there exists continuous families of solutions of the Euler equations with finite-area vortex patches in the exterior of the obstacle which, when the area of the vortex patches is decreased to zero with the circulation kept constant, approach one of the equilibrium solutions of the Föppl system [Figs. 1(c) and 1(d)]. Hence, each equilibrium solution of the classical Föppl system can be regarded as a singular limit of a family of Euler flows with finite-area symmetric vortex patches parametrized by the area of the vortex patch. Conversely, such Euler flows with finite-area vortex patches can be viewed as desingularizations of an equilibrium solution of the Föppl system with the same circulation. They will play an important role in this investigation and we will hereafter refer to them as the "EFHM flows." These flows are particularly relevant given our focus on wake flows, since flows with vortex patches with constant vorticity were proposed by Batchelor[5,6] as plausible models for steady wake flows in the high-Reynolds number limit. The goal of this investigation is to construct a family of "higher-order Föppl systems," i.e., a family of singular systems that will approximate with tunable accuracy the velocity field of a given EFHM flow. The motivation for this study comes from the area of flow control where simplified solutions of flow problems, the so-called reduced-order models, are needed for the design of algorithms based on methods of the control theory. The reason is that synthesis of even "simple" linear feedback control algorithms is a complex task which may easily lead to computationally intractable problems when applied to well-resolved discretizations of solutions of the governing equations.[7] On the other hand, the controller synthesis becomes much easier when the relevant properties of the system are distilled into a low-dimensional reduced-order model that can be used instead. It should be noted that construction of reduced-order models typically requires a complete solution of the governing equations which is simplified in the process. Such an approach was recently developed in Ref. 8 based on the classical Föppl system. The family of higher-order Föppl systems to be derived below will have the same dimension of the state space as the classical system, however, it will be characterized by an arbitrary number of adjustable parameters and will offer, therefore, more flexibility as a model for control design than the classical Föppl system does.

The higher-order Föppl systems will be constructed by expanding the complex potential induced by the vortex patches in an EFHM flow in a Taylor series with coefficients given in terms of moments of the vorticity in the vortex patches. We then look for equilibrium solutions of an order N truncation of such an expansion which will yield an Nth order Föppl system. The literature concerning solutions of the Euler equations involving finite-area vortex patches in both equilibrium and nonequilibrium configurations is abundant and we refer the reader to the monographs by Saffman[9]

[a)]Electronic mail: bprotas@mcmaster.ca

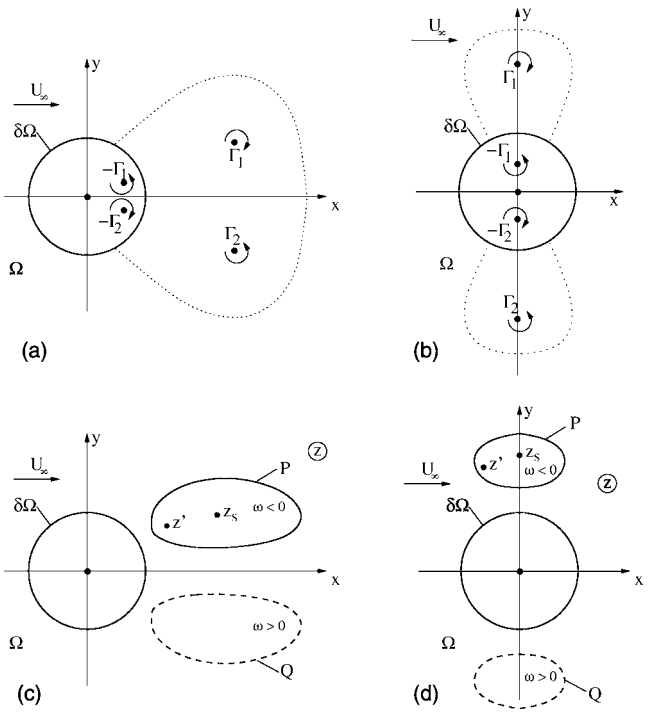

FIG. 1. Schematic showing two steady-state potential flow solutions for the cylinder wake flow together with their desingularizations: (a) the classical Föppl equilibrium and (c) the corresponding EFHM flow, (b) the equilibrium with vortices on the OY axis and (d) the corresponding EFHM flow. The dotted lines in (a) and (b) represent the separatrix streamlines delimiting the recirculation regions. The solid and dashed lines in (c) and (d) represent the boundaries of the regions with negative and positive vorticity.

and Newton[10] for a review. In the present context we specifically mention recent investigations by Crowdy, summarized in Ref. 11, which use advanced methods of complex analysis to develop an elegant formalism for calculation of equilibria involving vortex patches and multipolar vortices. The dynamics of vortex patches and of the corresponding point vortices in domains involving cylindrical obstacles was recently studied by Johnson and McDonald.[12] With regard to the use of moments of vorticity to characterize the evolution of a system of vortex patches, this approach was first employed by Melander, Zabusky, and Styczek[13,14] who showed that this representation has in fact the Hamiltonian structure. The approach we develop in this investigation is simpler, since higher-order moments of vorticity are not treated as additional degrees of freedom, but are used only to construct velocity fields better approximating the velocity in the flows with finite-area vortex patches.

The structure of this paper is as follows: in the next section we review the EFHM solutions and the classical Föppl equilibrium; in Sec. III we derive equations characterizing higher-order Föppl systems; in Sec. IV we study analytically and numerically the loci of the equilibrium solutions of the higher-order systems; stability properties of the new systems are discussed in Sec. V, whereas in Sec. VI we offer some comments regarding the relevance of the higher-order Föppl systems for flow control; final conclusions are deferred to Sec. VII.

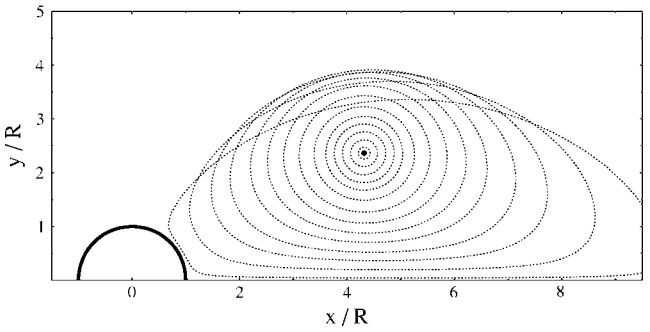

FIG. 2. Boundaries of the vortex patches with increasing area A obtained in the EFHM flows desingularizing the equilibrium solution (16) of the classical Föppl system (represented by a solid circle).

II. EFHM FLOWS AND THE CLASSICAL FÖPPL SYSTEM

In this section we briefly discuss the EFHM solutions[4] of the steady Euler equations and then characterize the Föppl equilibrium as a limit of a family of EFHM flows. The 2D steady-state Euler equations are equivalently expressed as[15]

$$\Delta\psi = f(\psi) \quad \text{in } \Omega,$$
$$\psi = 0 \quad \text{on } \partial\Omega, \tag{1}$$
$$\psi \to U_\infty y \quad \text{for } |(x,y)| \to \infty,$$

where ψ is the stream function, which allows the velocity components to be expressed as $u=\partial\psi/\partial y$ and $v=-\partial\psi/\partial x$, and f is an arbitrary function representing the relationship between the stream function and the vorticity ω as $\omega=f(\psi)$. In this investigation we are interested only in equilibrium solutions symmetric with respect to the flow centerline, so without loss of generality we can restrict Ω in (1) to the upper half-plane (i.e., corresponding to points with $y>0$). We note that the indeterminacy of the function f in (1) reflects the nonuniqueness of solutions of the Euler equations in a given domain Ω. The EFHM flows are obtained by prescribing a special form of the function $f(\Psi)$, namely

$$f(\psi) = \begin{cases} -\omega, & \psi \leqslant \alpha, \\ 0, & \psi > \alpha, \end{cases} \tag{2}$$

which corresponds to constant vorticity regions embedded in an irrotational flow. When $\alpha<0$, the vortex regions are *compact*, whereas when $\alpha>0$ the vortex regions are unbounded and extend to infinity. With regard to the first case, Elcrat *et al.*[4] showed that when the circulation of the vortex regions is kept constant, the solutions of (1) and (2) form families parametrized by the area of the vortex patches which approach the potential flow solutions with point-vortex singularities as the area of the vortex region is decreased to zero. In particular, one such family desingularizes the Föppl equilibrium (Fig. 2). In Fig. 3 we see that, as the area of the EFHM vortex region increases, the recirculation zone behind the obstacle becomes more elongated than in the classical Föppl system (cf. Ref. 8). Thus, the recirculation regions obtained in EFHM flows with larger vortex patches resemble more closely the actual flow patterns observed in steady-state

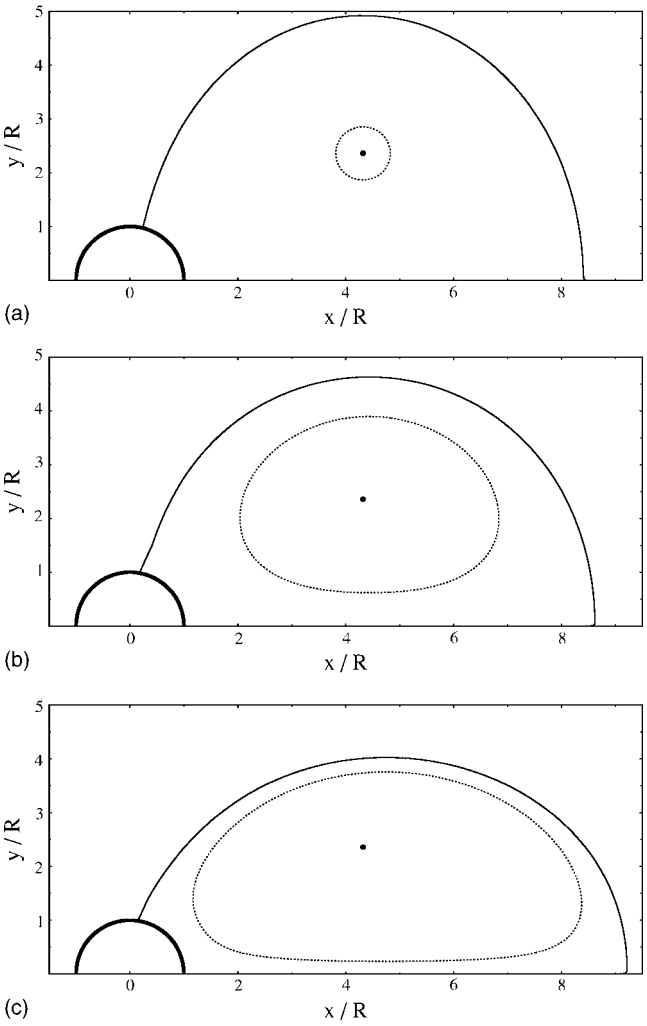

FIG. 3. (Solid lines) Boundaries of the recirculation regions and (dotted lines) boundaries of the corresponding vortex patches in the EFHM flows with the areas (a) $A=0.78$, (b) $A=12.55$, and (c) $A=20.43$ of the vortex region. The classical equilibrium (16) is marked with a solid circle, whereas the thick solid line represents the obstacle.

solutions of the Navier-Stokes system.[16] The classical equilibrium solutions of the Föppl system are obtained by taking the limit $\alpha \to -\infty$ in (2) which corresponds to representing the right-hand side of Eq. (1) as a linear combination of Dirac delta functions. The circulation Γ_0 and the position $z_0=x_0+iy_0$ (with $i=\sqrt{-1}$) of the singularities are related as

$$(|z_0|^2-R^2)^2=4|z_0|^2y_0^2,$$
$$\Gamma_0=-2\pi\frac{(|z_0|^2-R^2)^2(|z_0|^2+R^2)}{|z_0|^5}. \tag{3}$$

In addition to Föppl's original work,[1] elegant derivations of this result can be found in Kochin, Kibel, and Rose[17] and Milne-Thompson.[15] The complex potential corresponding to a Föppl equilibrium is given by

$$W_0(z)=W_C(z)+W_{F,0}(z), \tag{4}$$

where

$$W_C(z)=U_\infty\left(z+\frac{R^2}{z}\right), \tag{4a}$$

$$W_{F,0}(z)=\frac{\Gamma_0}{2\pi i}\left[\ln(z-z_0)-\ln\left(z-\frac{R^2}{\bar{z}_0}\right)-\ln(z-\bar{z}_0)+\ln\left(z-\frac{R^2}{z_0}\right)\right], \tag{4b}$$

with an overbar denoting complex conjugation. The complex velocity is obtained as $V_0(z)\triangleq dW_0(z)/dz$, where the symbol "$\triangleq$" will mean "equal to by definition." Equilibrium relations (3) then follow from the stationarity condition expressed using the complex velocity with the self-induction term subtracted off, i.e., $\hat{V}_0(z)\triangleq V_0(z)-\frac{\Gamma_0}{2\pi i}\frac{1}{z-z_0}=0$, which after some manipulation leads to the following factorized form:

$$\hat{V}_0(z_0)=\frac{P_0(z_0,\bar{z}_0)}{z_0^2|z_0|^2(|z_0|^2+R^2)Q(z_0,\bar{z}_0)}$$
$$\triangleq\frac{-\dfrac{iR^2\Gamma}{2\pi}(z_0^2|z_0|^2-\Theta)(z_0^2|z_0|^2-\bar{\Theta})}{z_0^2|z_0|^2(|z_0|^2+R^2)(z_0-\bar{z}_0)(|z_0|^2-R^2)(z_0^2-R^2)}$$
$$=0, \tag{5}$$

where

$$\Theta=\frac{1}{2}[|z_0|^4+2|z_0|^2R^2-R^4+i(|z_0|^2-R^2)\sqrt{3|z_0|^4+2|z_0|^2R^2-R^4}].$$

Expression (5) makes it evident that $\hat{V}_0(z)$ vanishes at the two points characterized by the relations $z_0|z_0|=\sqrt{\Theta}$ and $z_0|z_0|=\sqrt{\bar{\Theta}}$ which are precisely the Föppl equilibrium (3) and its reflection with respect to the OX axis. We remark that in deriving expression (5) it is assumed that $x_0\neq 0$, hence the factorized form does not apply to the other family of equilibrium solutions of the Föppl systems for which $x_0\equiv 0$ [Fig. 1(b)].

III. HIGHER-ORDER FÖPPL SYSTEMS

In this section we derive a family of equations characterizing higher-order corrections to the classical Föppl equilibrium (3) and corresponding to the EFHM flows desingularizing this equilibrium with finite-area vortex regions. We will accomplish this by considering the complex potential induced by a system of vortex patches in an EFHM flow and then expanding it in a Taylor series about a point z_s, or its conjugate $\bar{z}_s$, located inside the vortex regions, respectively, P and Q, where Q is a mirror reflection of the vortex region P in the lower half-plane [Fig. 1(c)]. This expansion will then be truncated at some finite order N and the center of expansion z_s will be determined as an equilibrium of the truncated system. Using the complex Green's function for the Laplace equation in a 2D unbounded domain $G(z,z')=1/(2\pi i)\ln(z-z')$ and noting that the vorticity distribution

in an EFHM flow is by construction antisymmetric with respect to the OX axis, we obtain the following expression for the complex potential:

$$\tilde{W}_P(z) = \frac{1}{2\pi i}\int_P [\ln(z-z')\omega(z') + \ln(z-\bar{z}')\omega(\bar{z}')]dA(z'), \tag{6}$$

where the tilde $\tilde{(\cdot)}$ indicates that the potential represents a flow in an unbounded domain (i.e., without an obstacle). The integration domain P extends over vortex region(s) in the upper half-plane (i.e., the vortex patch P) and $dA(z') = dx'dy'$. We note that expression (6) is valid for $z \notin P$ and $z \notin Q$. We now choose $z_s \in P$ as the origin of a local coordinate system associated with the patch P and set $\zeta = z' - z_s$ [see Fig. 1(c)]. By symmetry, we will also have $\bar{z}'$, $\bar{z}_s \in Q$. The complex potential (6) can now be expressed as

$$\begin{aligned}\tilde{W}_P(z) = {} & \frac{\Gamma_0}{2\pi i}\ln(z-z_s) - \frac{\Gamma_0}{2\pi i}\ln(z-\bar{z}_s) \\ & + \frac{1}{2\pi i}\int_P \left[\ln\left(1-\frac{\zeta}{z-z_s}\right)\omega(z_s+\zeta) \right. \\ & \left. + \ln\left(1-\frac{\bar{\zeta}}{z-\bar{z}_s}\right)\omega(\bar{z}_s+\bar{\zeta})\right] dA(\zeta).\end{aligned} \tag{7}$$

The third term in (7) can, for $|z-z_s| > |z'-z_s|$, be expanded in a Taylor series which yields

$$\begin{aligned}\tilde{W}_P(z;z_s) = {} & \frac{\Gamma_0}{2\pi i}\ln\frac{(z-z_s)}{(z-\bar{z}_s)} \\ & - \frac{1}{2\pi i}\sum_{n=1}^{\infty}\frac{1}{n}\left[\frac{c_n(z_s)}{(z-z_s)^n} - \frac{\bar{c}_n(\bar{z}_s)}{(z-\bar{z}_s)^n}\right], \quad |z-z_s| > \zeta_m,\end{aligned} \tag{8}$$

where

$$c_n(z_s) = \int_P \omega(z_s+\zeta)\zeta^n dA(\zeta) \tag{9}$$

and $\zeta_m = \max_{(z_s+\zeta)\in P}|\zeta|$. The second argument in the expression for $\tilde{W}_P(\cdot;\cdot)$ represents the center of expansion which, for the moment, remains unspecified. The quantities $c_n(z_s)$, $n=0,1,\ldots$, are the moments of the vorticity distribution in the patch P with respect to the point z_s and therefore are related to the total circulation of the patch ($c_0 \equiv \Gamma$), its eccentricity (c_1), its ellipticity (c_2), etc. (unless required for clarity, hereafter we will skip the argument of c_n). The vorticity distribution inside the vortex region P being uniform, the infinite set of moments c_n, $n=0,1,\ldots$, encodes the information about the shape of the region P. As a matter of fact, this is a well-known device of mathematical analysis (see, for instance, the monograph by Akhiezer and Krein[18]) which can also be used to reconstruct planar domains based on their moments.[19] In fluid mechanics, Melander, Zabusky, and Styczek[13,14] were the first to use sets of vorticity moments as state variables for solution of the 2D Euler equations (see the monographs by Saffman[9] and Newton[10] for a survey and additional references). As compared to this method, the present approach is simpler, since the vorticity moments are not treated as independent dynamic variables, but are used only to obtain a better approximation of the velocity field in the corresponding EFHM flow. In order to obtain a finite system we now truncate expression (8) and retain terms up to the order N (the truncation order will be indicated by a subscript on W)

$$\begin{aligned}\tilde{W}_P(z;z_s) \cong \tilde{W}_{P,N}(z;z_s) = {} & \frac{\Gamma_0}{2\pi i}\ln\frac{(z-z_s)}{(z-\bar{z}_s)} \\ & - \frac{1}{2\pi i}\sum_{n=1}^{N}\frac{1}{n}\left[\frac{c_n(z_s)}{(z-z_s)^n} - \frac{\bar{c}_n(\bar{z}_s)}{(z-\bar{z}_s)^n}\right],\end{aligned}$$

$$|z-z_s| > \zeta_m. \tag{10}$$

The truncated expression (10) represents the potential in an unbounded domain. In order to obtain the potential in the corresponding flow past a cylindrical obstacle, we need to include the potential W_C representing the basic potential flow past a circular cylinder (4a) and also need to ensure that the boundary conditions for the wall-normal velocity component are satisfied on the boundary $\delta\Omega$. This is done by invoking the "Circle Theorem"[15] which states that if $\tilde{w}(z)$ is the complex potential of a flow in a domain without boundaries and with singularities at some points z_k such that $\forall k$, $|z_k| > R$, then the complex potential of the corresponding flow past the cylinder with radius R is given by the expression $w(z) = \tilde{w}(z) + \bar{\tilde{w}}(R^2/z)$. The second term in the expression for $w(z)$ represents "image singularities" located inside the obstacle. Thus, after including W_C and the image singularities, the complete truncated potential is now

$$\begin{aligned}W_N(z;z_s) = {} & W_C(z) + \tilde{W}_N(z;z_s) + \bar{\tilde{W}}_N\left(\frac{R^2}{z};z_s\right) \\ = {} & U_\infty\left(z+\frac{R^2}{z}\right) + \frac{\Gamma_0}{2\pi i}\left[\ln(z-z_s) - \ln\left(z-\frac{R^2}{\bar{z}_s}\right) - \ln(z-\bar{z}_s) + \ln\left(z-\frac{R^2}{z_s}\right)\right] \\ & + \frac{1}{2\pi i}\sum_{n=1}^{N}\frac{1}{n}\left[\frac{c_n(z_s)}{(z-z_s)^n} - (-1)^n\frac{\bar{c}_n(\bar{z}_s)}{\left(z-\frac{R^2}{\bar{z}_s}\right)^n}\left(\frac{z}{\bar{z}_s}\right)^n - \frac{\bar{c}_n(\bar{z}_s)}{(z-\bar{z}_s)^n} + (-1)^n\frac{c_n(z_s)}{\left(z-\frac{R^2}{z_s}\right)^n}\left(\frac{z}{z_s}\right)^n\right].\end{aligned} \tag{11}$$

We notice that setting $N=0$ in (11) we recover complex potential (4) of the classical Föppl system discussed in Sec. I. Therefore, the family of the complex potentials given in (11) represents Nth order corrections to the Föppl system regarded as approximations of the corresponding solution of the steady-state Euler equations and hereafter we will refer to them as "Nth order Föppl systems." By taking N large enough we can obtain an arbitrarily accurate representation of the potential and other related quantities (such as the velocity) in the Euler flow valid for points in the flow domain outside the vortex patches.

We proceed to characterize equilibria z_N of the Nth order Föppl system (11), i.e., positions of the expansion centers z_s which do not move under the induction of the system. The advection velocity is obtained by subtracting off all the self-induction terms (i.e., the terms which become singular as $z \to z_s$)

$$\hat{V}_N(z;z_s) \triangleq V_N(z;z_s) - \frac{1}{2\pi i}\left[\frac{\Gamma_0}{z-z_s} - \sum_{n=1}^{N}\frac{c_n(z_s)}{(z-z_s)^{n+1}}\right], \tag{12}$$

where $V_N(z;z_s)=dW_N(z;z_s)/dz$. Thus, for every N, the stationarity condition characterizing a higher-order equilibrium z_N is given by

$$\hat{V}_N(z_N;z_N)=0. \tag{13}$$

Before we expand this expression, let us make explicit the dependence of the moments $c_n(z_s)$, $n=1,\ldots,N$, on z_s. We do this by introducing another arbitrary center of expansion, for example z_0 [cf. (3)], so that $z_s=z_0+(z_s-z_0)$ and using the binomial theorem we can rewrite (9) as

$$c_n(z_s)=\sum_{q=0}^{n}\binom{n}{q}(z_0-z_s)^{(n-q)}c_q(z_0), \quad n=0,\ldots,N. \tag{14}$$

Thus, given the moments $c_n(z_0)$, $n=1,\ldots,N$, calculated with respect to some point (here z_0), the Nth order moment $c_n(z_s)$ with respect to z_s can be expressed as an Nth order polynomial in z_s with coefficients given in terms of the moments $c_n(z_0)$. This observation allows us to expand condition (13) as follows:

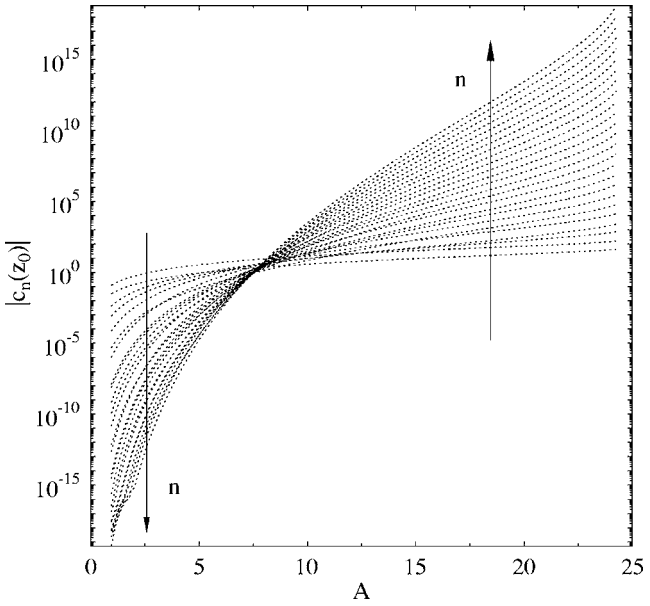

FIG. 4. The magnitudes of the moments $c_n(z_0)$ for $n=1,\ldots,25$ as a function of the area A of the vortex region in the EFHM flow. The arrows indicate the trends corresponding to an increase of the order n of the moment for small and large parches (cf. Fig. 2).

$$\begin{aligned}\hat{V}_N(z_N;z_N) = {} & U_\infty\left(1-\frac{R^2}{z_N^2}\right)+\frac{\Gamma_0}{2\pi i}\left[-\frac{1}{\left(z_N-\frac{R^2}{\bar{z}_N}\right)}-\frac{1}{(z_N-\bar{z}_N)}+\frac{1}{\left(z_N-\frac{R^2}{z_N}\right)}\right]\\ & -\frac{1}{2\pi i}\sum_{n=1}^{N}\left\{\left[\sum_{q=0}^{n}\binom{n}{q}(\bar{z}_0-\bar{z}_N)^{(n-q)}\bar{c}_q(z_0)\right]\left[\frac{(-1)^{n+1}R^2}{\left(z_N-\frac{R^2}{\bar{z}_N}\right)^{n+1}}\frac{z_N^{n-1}}{\bar{z}_N^{n+1}}-\frac{1}{(z_N-\bar{z}_N)^{n+1}}\right]\right.\\ & \left.-\left[\sum_{q=0}^{n}\binom{n}{q}(z_0-z_N)^{(n-q)}c_q(z_0)\right]\frac{(-1)^{n+1}R^2}{\left(z_N-\frac{R^2}{z_N}\right)^{n+1}}\frac{1}{z_N^2}\right\}=0,\end{aligned} \tag{15}$$

which, for every truncation order N, represents a complex algebraic equation characterizing an Nth order equilibrium z_N.

IV. EQUILIBRIA OF THE HIGHER-ORDER SYSTEMS

In this section we study certain properties of the higher-order equilibria governed by Eq. (15). Evidently, these equilibria depend on two parameters: the truncation order N, which is a discrete parameter, and the set of moments $c_n(z_0)$, $n=1,\ldots,N$, which vary continuously with the area A of the EFHM vortex region desingularizing the classical equilibrium (3) (Fig. 4). We will first make use of certain well-known facts from algebraic geometry to state some general qualitative properties of the loci of the higher-order equilibria as a function of the two parameters. Then we will use numerical computations to characterize these loci quantitatively. To fix attention, in all the calculations we will focus on desingularizations of the classical Föppl equilibrium given by

$$z_0 = x_0 + iy_0 = 4.32 + i2.3596, \qquad \Gamma_0 = -29.6015. \tag{16}$$

(This is the equilibrium that was investigated in Ref. 8.)

Using factorization (5) and bringing the different rational fractions to a common denominator, expression (15) corresponding to different truncation orders can be rewritten as the following recursively defined hierarchy of conditions:

$$\hat{V}_1(z_1;z_1) = \frac{P_0(z_1,\bar{z}_1)Q(z_1,\bar{z}_1) + \bar{c}_1(\bar{z}_1)K_1(z_1,\bar{z}_1) + c_1(z_1)L_1(z_1,\bar{z}_1)}{z_1^2|z_1|^2(|z_1|^2+R^2)Q(z_1,\bar{z}_1)} \triangleq \frac{P_1(z_1,\bar{z}_1)}{z_1^2|z_1|^2(|z_1|^2+R^2)Q(z_1,\bar{z}_1)} = 0, \tag{17a}$$

$$\hat{V}_2(z_2;z_2) = \frac{P_1(z_2,\bar{z}_2)Q(z_2,\bar{z}_2) + \bar{c}_2(\bar{z}_2)K_2(z_2,\bar{z}_2) + c_2(z_2)L_2(z_2,\bar{z}_2)}{z_2^2|z_2|^2(|z_2|^2+R^2)Q^2(z_2,\bar{z}_2)} \triangleq \frac{P_2(z_2,\bar{z}_2)}{z_2^2|z_2|^2(|z_2|^2+R^2)Q^2(z_2,\bar{z}_2)} = 0, \tag{17b}$$

$$\ldots$$

$$\ldots$$

$$\hat{V}_N(z_N;z_N) = \frac{P_{N-1}(z_N,\bar{z}_N)Q(z_N,\bar{z}_N) + \bar{c}_N(\bar{z}_N)K_N(z_N,\bar{z}_N) + c_N(z_N)L_N(z_N,\bar{z}_N)}{z_N^2|z_N|^2(|z_N|^2+R^2)Q^N(z_N,\bar{z}_N)} \triangleq \frac{P_N(z_N,\bar{z}_N)}{z_N^2|z_N|^2(|z_N|^2+R^2)Q^N(z_N,\bar{z}_N)} = 0, \tag{17c}$$

where $P_0(z,\bar{z})$ and $Q(z,\bar{z})$ are polynomials (in z and $\bar{z}$) of the total degree 8 and 5, respectively, defined in (5). The polynomials $K_n(z,\bar{z})$ and $L_n(z,\bar{z})$, $n=1,2,\ldots$, are given by

$$K_n(z,\bar{z}) \triangleq z^3\bar{z}(z\bar{z}+R^2)(z^2-R^2)^{n+1}[(z\bar{z}-R^2)^{n+1} - R^2z^{n-1}(z-\bar{z})^{n+1}], \tag{18a}$$

$$L_n(z,\bar{z}) \triangleq R^2z^{n+1}\bar{z}(z\bar{z}+R^2)(z\bar{z}-R^2)^{n+1}(z-\bar{z})^{n+1}, \tag{18b}$$

hence their degree is, respectively, $\deg[K_n(z,\bar{z})]=4n+10$ and $\deg[L_n(z,\bar{z})]=4n+8$. We emphasize that, by (14), the factors $c_n(z)$ and $\bar{c}_n(\bar{z})$ are also polynomials of order n in z and $\bar{z}$, respectively. We note that each of the conditions in hierarchy (17) is defined recursively in terms of the condition corresponding to the next lower truncation order. We see that, for given N and $c_n(z_0)$, $n=1,\ldots,N$, condition (17c) is equivalent to $P_N(z_N,\bar{z}_N)=0$ which can be expressed as a system of two real polynomial equations in x and y

$$p_N(x_N,y_N) \triangleq \Re[P_N(x_N+iy_N,x_N+iy_N)] = p_N^0(x_N,y_N) + p'_N(x_N,y_N) = 0,$$
$$q_N(x_N,y_N) \triangleq \Im[P_N(x_N+iy_N,x_N+iy_N)] = q_N^0(x_N,y_N) + q'_N(x_N,y_N) = 0, \tag{19}$$

where $\deg[p'_N(x,y)] \geqslant \deg[p_N^0(x,y)]$ and $\deg[q'_N(x,y)] \geqslant \deg[q_N^0(x,y)]$. The polynomials $p_N^0(x,y)$ and $q_N^0(x,y)$ are related to the term in $P_N(z,\bar{z})$ involving $P_{N-1}(z,\bar{z})$ as a factor and therefore vanish at all the roots of the corresponding polynomials of the lower degree, i.e., $p_{N-1}^0(x,y)$ and $q_{N-1}^0(x,y)$. The polynomials $p'_N(x,y)$ and $q'_N(x,y)$ have degrees higher than $p_N^0(x,y)$ and $q_N^0(x,y)$, because they represent the "perturbation" corresponding to an increase of the order of truncation. Evidently, solutions of (19) represent intersection points of two algebraic curves in the plane. The problem of determining intersection points of two algebraic curves belongs to the area of computational algebraic geometry. There are many profound results in this field (see Ref. 26 for a recent review), however, for our purposes here we will need some basic facts only.

First, we are interested in how the locus of the higher-

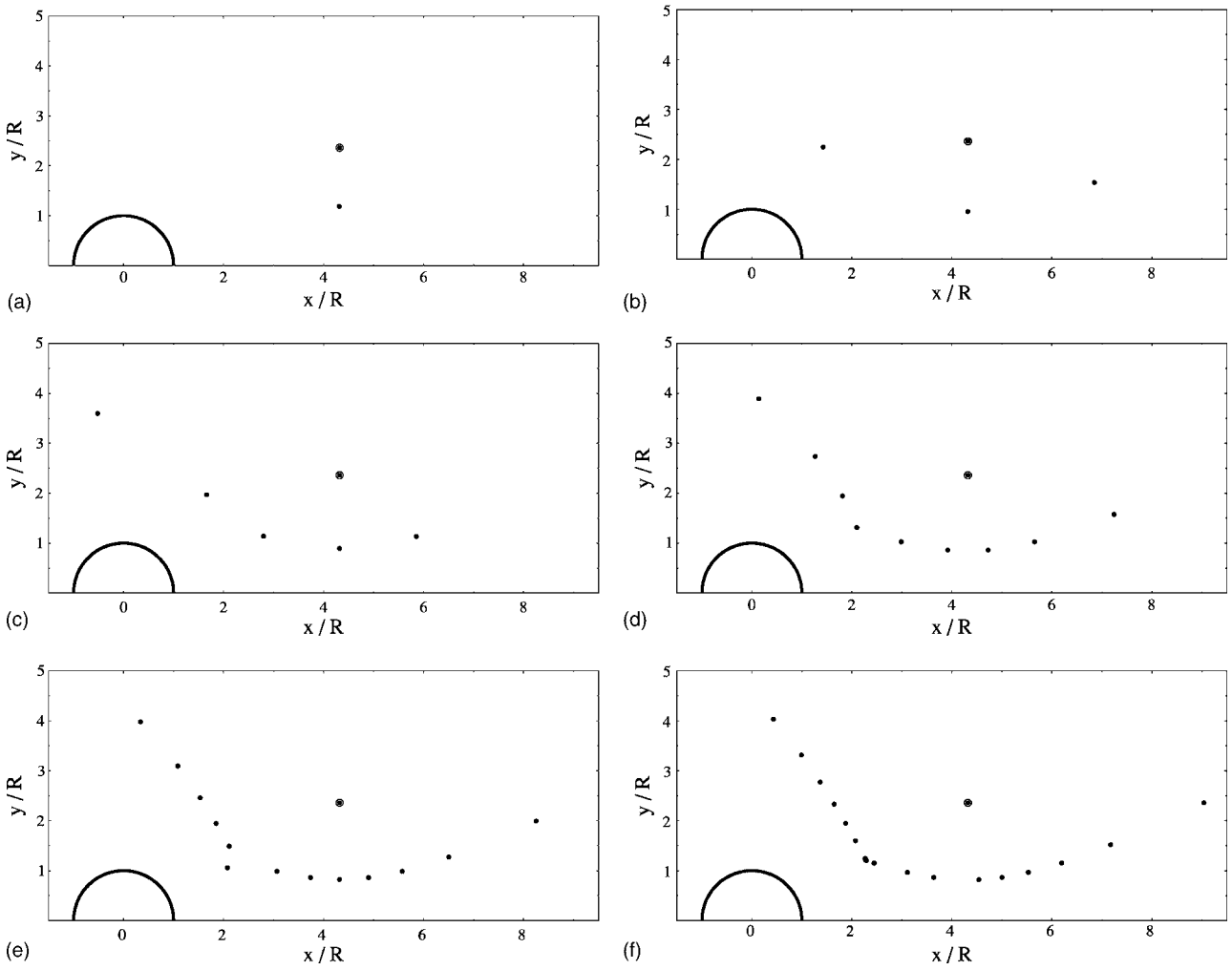

FIG. 5. Loci of the higher-order equilibria of order (a) $N=1$, (b) $N=3$, (c) $N=5$, (d) $N=10$, (e) $N=15$, (f) $N=20$ corresponding to the case $A=0$. The classical equilibrium (16) is marked with a larger circle, whereas the thick solid line represents the obstacle.

order equilibria depends on the truncation order N. The Bézout theorem[20] states that, given two polynomials $p(x,y)$ and $q(x,y)$, the number of roots they have in common (counting multiplicities) in the projective plane is $\deg[p(x,y)]\cdot\deg[q(x,y)]$ [in fact, the number of roots actually found in the (x,y) plane is for many algebraic curves much smaller]. Thus, the upper bound on the number of equilibrium solutions increases with the truncation order N as $\mathcal{O}(N^2)$. In order to say something about the locus of these equilibrium solutions, we have to fix the second parameter, i.e., the vortex patch area A and hence also the corresponding moments $c_n(z_0)$, $n=1,2,\ldots$. For simplicity, we choose

$$A=0, \quad \text{so that } c_n(z_0)\equiv 0, \quad n=1,2,\ldots \tag{20}$$

[even though in this case the EFHM flow coincides with the classical Föppl equilibrium (3), we can still formally define the higher-order system (15)]. We note that expression (14) for the moments now takes a particularly simple form

$$c_n(z)=(z-z_0)^n c_0(z_0)=(z-z_0)^n\Gamma, \quad n=1,2,\ldots. \tag{21}$$

We can now state the following Lemma:

Lemma 1: When condition (20) holds, the classical equilibrium (3) is also a solution of a higher-order system (15) for arbitrary N.

Proof: Setting $z_n=z_0$ and using (20) and (21) we note that all terms involving $K_n(z_n,\bar{z}_n)$ and $L_n(z_n,\bar{z}_n)$, $n=1,\ldots,N$, in (17) vanish. Hence, condition (17c) reduces to $P_0(z_N,\bar{z}_N)Q(z_N,\bar{z}_N)^N=0$ which is equivalent to (5). Thus, when $A=0$, z_0 is a higher-order equilibrium of arbitrary order. □

With regard to new roots appearing in the higher-order system, we note that the coefficients of the highest-order terms in (19) are proportional to Γ [cf. (21)], and therefore nonvanishing when $A\to 0$. Thus, referring to standard estimates of the maximum magnitude of roots of a polynomial in terms of its coefficients,[27] we conclude that the magnitudes of the new roots should be bounded as $A\to 0$. The locus of the roots corresponding to different truncation orders N when $A=0$ is shown in Fig. 5 (these roots were determined numerically and some details regarding computations are given below). We observe that, except for the persistent classical equilibrium (16), all of the remaining higher-order equilibria fall on a curved band which separates the classical equilibrium from the obstacle. As a matter of

fact, all of the higher-order equilibria other than (16) will result in a singularity of the velocity field in the part of the flow domain where it is required to by analytic, i.e., outside of the vortex patch which is now reduced to a point. Hence, we will consider all these additional equilibria spurious (unphysical), and will not investigate them below.

We now proceed to analyze the dependence of the higher-order equilibria on the area A of the vortex region. As shown in Fig. 4, when the vortex region shrinks to a point, the moments $c_n(z_0)$, $n=1,\ldots,N$ vanish. From (14) and (17) we conclude that coefficients of polynomials (19) are affine functions of the moments $c_n(z_0)$, hence continuous dependence of the equilibrium solutions on the moments is ensured by the following generalization of the Fundamental Continuity Theorem for polynomials[20] for the case of the systems of two polynomials:

Theorem 2: *Suppose there are two sequences of projective plane curves* $C_n(x,y)$ *and* $D_n(x,y)$ *such that* $deg[C_n(x,y)]$ *and* $deg[D_n(x,y)]$ *are constant. Assume the sequences have limits* $C(x,y)$ *and* $D(x,y)$. *Then each intersection point of* $C(x,y)$ *and* $D(x,y)$ *is the limit of as many intersection points (counted with multiplicities) of* $C_n(x,y)$ *and* $D_n(x,y)$ *as the local intersection multiplicity of* $C(x,y)$ *and* $D(x,y)$ *at that point*.

A sketch of a proof of this Theorem is deferred to the Appendix.

Hence, based on Lemma 1 and Theorem 2, we can conclude that as the area of the EFHM vortex region desingularizing the classical equilibrium (3) goes to zero, for every truncation order N there will exist a family of higher-order equilibria converging to the classical equilibrium (3). In fact, the same will also hold for the spurious equilibria.

Now we illustrate our findings in a quantitative manner using numerical computations. For a set of truncation orders $N=\{1,\ldots,25\}$ we will calculate the loci of the equilibrium solutions z_N corresponding to EFHM flows with areas of the vortex region growing from zero to the largest value for which an EFHM solution can still be found (the version of the code calculating the EFHM flows that we have at our disposal does not make it possible to find solutions with vortex regions attached to the obstacle, cf. Fig. 2). In every instance, Eq. (15) is solved using Newton's method[21] and a simple continuation approach ensures that the roots found belong in fact to the branch starting with the classical Föppl equilibrium (3). Numerical calculation of moments is facilitated by transforming the area integral appearing in expression (9) into a contour integral using the complex Green's theorem

$$c_n(z_0)=\omega\int_P \zeta^n dA(\zeta)=\frac{i\omega}{2(n+1)}\oint_{\partial P}\zeta^{(n+1)}d\bar{\zeta}, \tag{22}$$

where ∂P denotes the boundary of the patch P. All numerical results presented below were tested for convergence using different numerical resolutions employed to compute the EFHM flows. The loci parametrized by the area of the EFHM vortex regions and corresponding to several different truncation orders N are shown in Figs. 6(a) and 6(b). We note that with increasing area of the vortex region, the higher-order equilibria are initially shifted downstream. When the vortex region is large enough, it begins to significantly deform as a result of interaction with the obstacle. This trend is reflected more strongly in the higher-order moments (Fig. 4), hence the loci of the equilibrium solutions corresponding to truncations at higher orders ($N\gtrsim 5$) have more complicated shapes. In Fig. 6(b) we observe that the loci corresponding to $N=5,10,15$ are characterized by sharp lobes indicating that at some point the equilibrium positions start to move upstream with the increase of the area of the vortex region. In Fig. 7(a) we show the loci of the equilibrium solutions parametrized by the truncation order N and corresponding to three representative EFHM flows with different areas of the vortex regions. We note that these loci reveal certain similarities, namely for $N\to N_{\max}=25$ the equilibrium solutions z_N tend to "accumulation points" $z_{N_{\max}}=x_{N_{\max}}+iy_{N_{\max}}$. In order to emphasize some generic features of these loci, in Figs. 7(b)–7(d) the loci are plotted after the following change of variables:

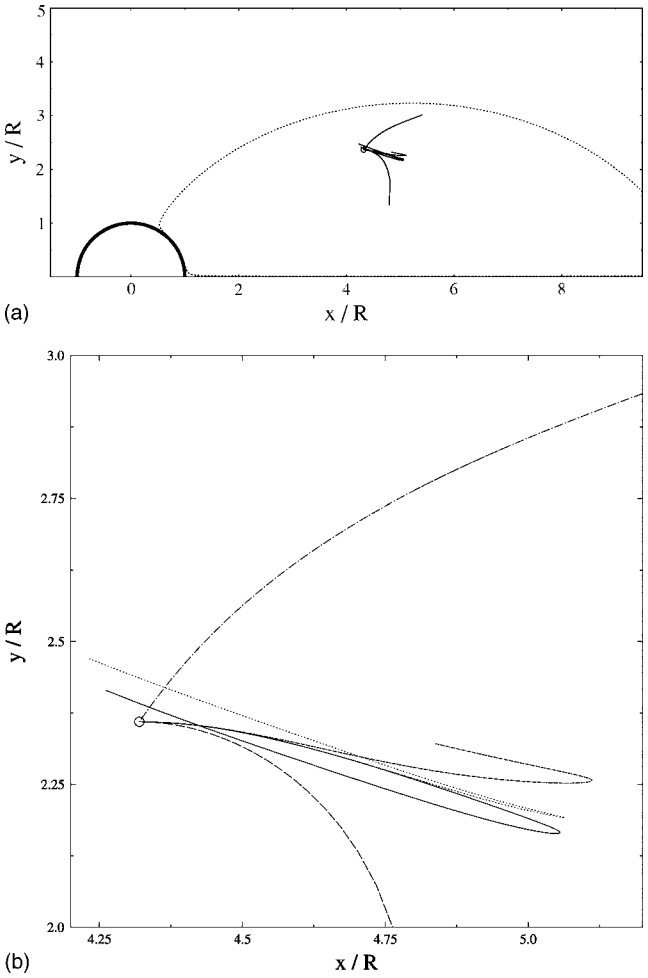

FIG. 6. Loci of the higher-order equilibria parametrized by the area of the vortex region in the EFHM flow for different truncation orders: (dashed-dotted) $N=1$, (long dashed) $N=3$, (short dashed) $N=5$, (dotted) $N=10$, (solid) $N=15$. [In (a) the solid line is used for all orders.] (b) Represents a magnification of the neighborhood of the classical Föppl equilibrium (16) which is indicated by an open circle. The dotted line in (a) represents the boundary of the largest vortex region obtained in an EFHM flow (with $A=24.33$), whereas the thick solid line represents the obstacle.

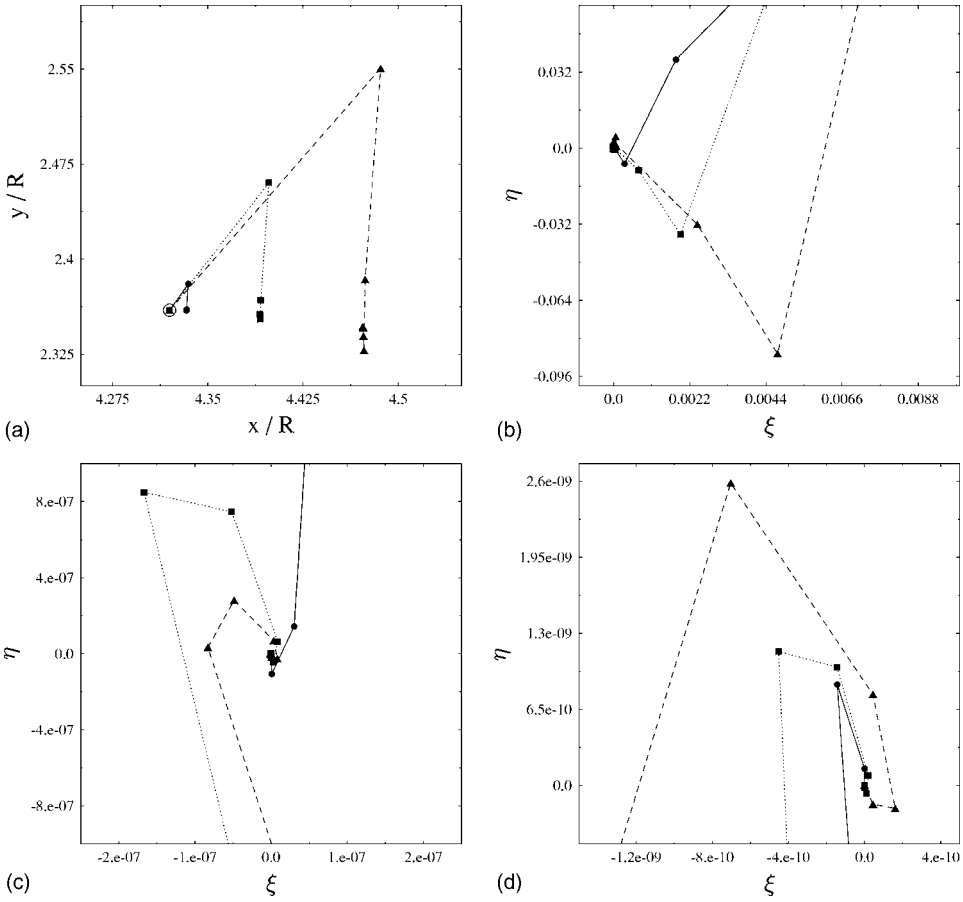

FIG. 7. Loci of the equilibrium solutions parametrized by the truncation order N (with $N_{\max}=25$) and corresponding to the EFHM flows with the following areas of the vortex regions: (solid line+circles) $A=4.51$, (dotted line+squares) $A=9.99$, and (dashed line+triangles) $A=13.88$. (a) Shows the neighborhood of the classical Föppl equilibrium (16) which is marked with an open circle. Figures (b)–(d) use transformation (23) and different ranges of the ξ and η coordinates.

$$\xi + i\eta = \frac{z - z_{N_{\max}}}{r}, \tag{23}$$

where $r \triangleq \max_n\{|x_n - x_{N_{\max}}|, |y_n - y_{N_{\max}}|\}$. This change of variables shifts the origin to the accumulation point of a given locus and normalizes its "size." We note that in all cases the rescaled loci reveal a spiraling pattern as the accumulation point is approached. As the intervals shown in Figs. 7(b)–7(d) indicate, this behavior persists across nine orders of magnitude. In fact, it appears to be only limited by the finite-precision arithmetic used to solve system (15) and the numerical resolution employed to compute the EFHM flows [numerical resolution must increase with the order of moments $c_n(z_0)$ that have to be calculated].

We conclude this section by analyzing how the velocity field $V_N(z)=(u_N - iv_N)(z)$ generated by an Nth order Föppl system approaches for increasing N the velocity field in the corresponding EFHM flow. In Fig. 8 we show the longitudinal velocity profiles $u_N(x)$ and the absolute errors $|u_N(x) - u(x)|$ with respect to the EFHM solutions $u(x)$ as a function of $z=x+i0$ on the flow centerline for different truncation orders N and three representative values of the area A. We observe that in the case of the small patch u_N converges to u everywhere on the flow centerline [Fig. 8(a)] and this convergence is fairly rapid. On the other hand, for the case of the medium and large patches there exist intervals $I_0 \in \mathbb{R}$ where convergence does not occur. The reason is that the points in I_0 do not satisfy the condition $|z - z_N| > \zeta_m$ necessary for convergence of expansion (10). However, even though for $x \in I_0$ the errors $|u_N(x,0) - u(x,0)|$ can be fairly large, when $x \notin I_0$ convergence is fast. Given this rapid convergence of the velocity fields in higher-order Föppl equilibria with the truncation order N, the corresponding flow patterns are for all $N \geqslant 1$ quite similar to the flow patterns in the EFHM flows with the same area A of the vortex region (cf. Fig. 3) and therefore are not shown here.

V. STABILITY OF THE HIGHER-ORDER SYSTEM

This section is devoted to the linear stability analysis of the higher-order equilibria discussed in Sec. IV. The linear stability of the classical Föppl system was investigated by several researchers including Föppl himself,[1] Smith,[22] Cai *et al.*,[23] and de Laat and Coene.[24] A summary of the most important results together with their derivation can be found in Tang and Aubry.[25] We emphasize that, in contrast to the symmetric equilibrium solutions, solutions of the time-dependent Föppl system are not assumed to possess any symmetries. Therefore, the Föppl model, either classical or higher-order, is a four-dimensional dynamical system. In general, the eigenvalues of its linearization around the corresponding equilibrium, i.e., either classical z_0, or higher-order z_N, form the following set:

$$\{\lambda_{r-}, \lambda_{r+}, \lambda_c, \bar{\lambda}_c\}, \quad \text{where: } -\lambda_{r-}, \lambda_{r+} \in \mathbb{R}^+, \quad \lambda_c \in \mathbb{C}. \tag{24}$$

For the classical Föppl system we additionally have $\lambda_{r-} = -\lambda_{r+}$ and $\Re(\lambda_c) = 0$ (in this case all the eigenvalues are

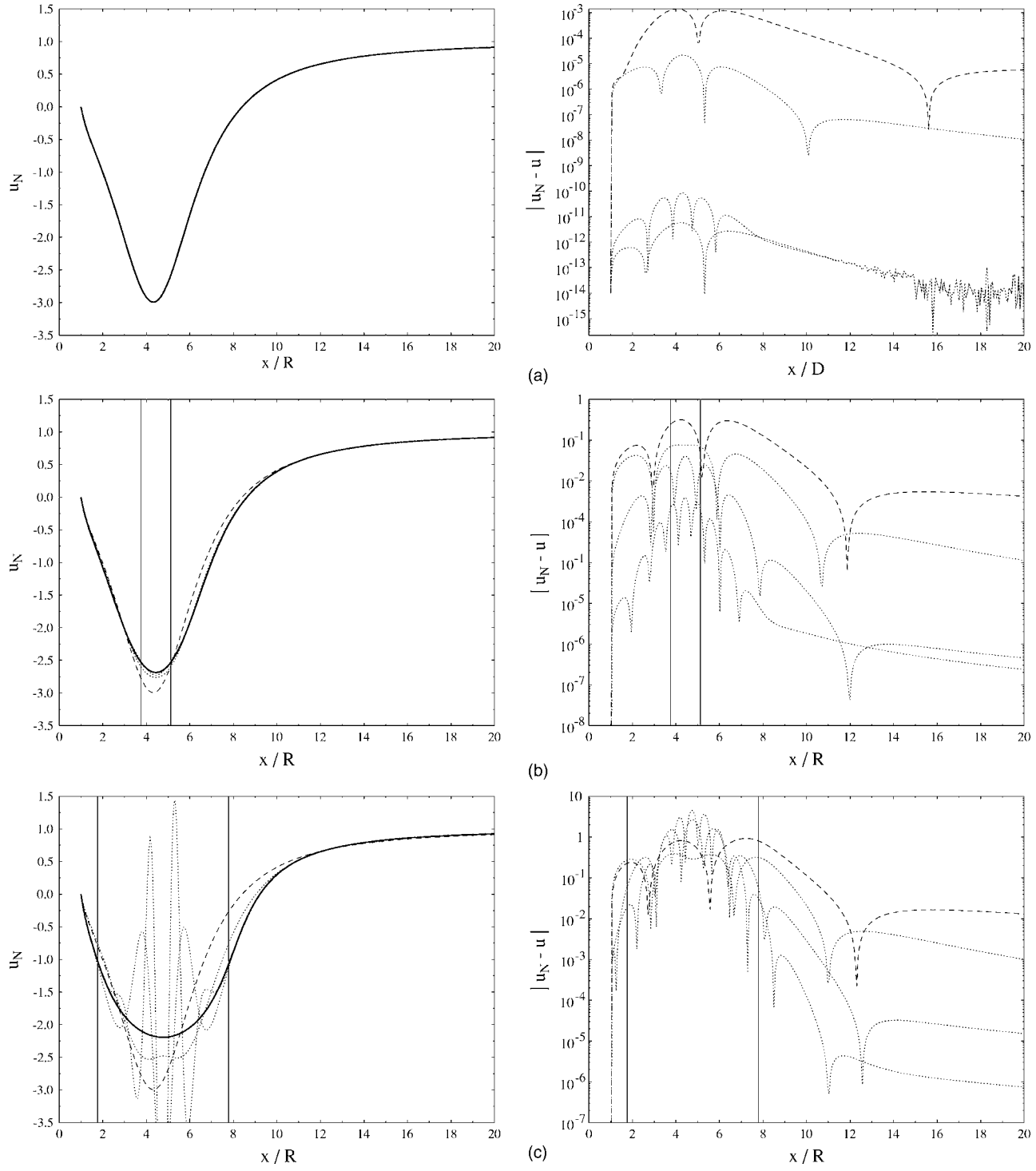

FIG. 8. Plots of (left) the longitudinal velocity $u_N(x)$ and (right) the difference $|u_N(x)-u(x)|$ between this velocity and the velocity in the corresponding EFHM flow on the centerline obtained in: (dashed line) the classical Föppl system and (dotted lines) higher-order Föppl systems with $N=2,6,10$ [lines closer to the EFHM solutions (left), or exhibiting lower errors (right), correspond to higher N]. The three cases correspond to (a) $A=0.78$, (b) $A=12.55$, and (c) $A=20.43$. The thick solid lines in the figures on the left represent $u(x)$ in the EFHM solutions with the corresponding patch. The vertical lines in (b) and (c) represent the bounds of the interval I_0.

in fact available in an analytic form). Thus, the linearization of the classical Föppl system around equilibrium (3) has three eigenmodes: a exponentially growing mode (associated with λ_{r+}), an exponentially decaying mode (associated with λ_{r-}), and a neutrally stable oscillatory mode (associated with the conjugate pair $\{\lambda_c,\bar{\lambda}_c\}$). We now analyze how the eigenvalue structure changes in linearizations of the higher-order Föppl systems depending on the two parameters, namely, the truncation order N and the area A of the EFHM vortex region used to desingularize equilibrium (16). In all cases the set of eigenvalues has the same general form as given in (24). In Figs. 9(a)–9(d) we show the dependence of the four relevant

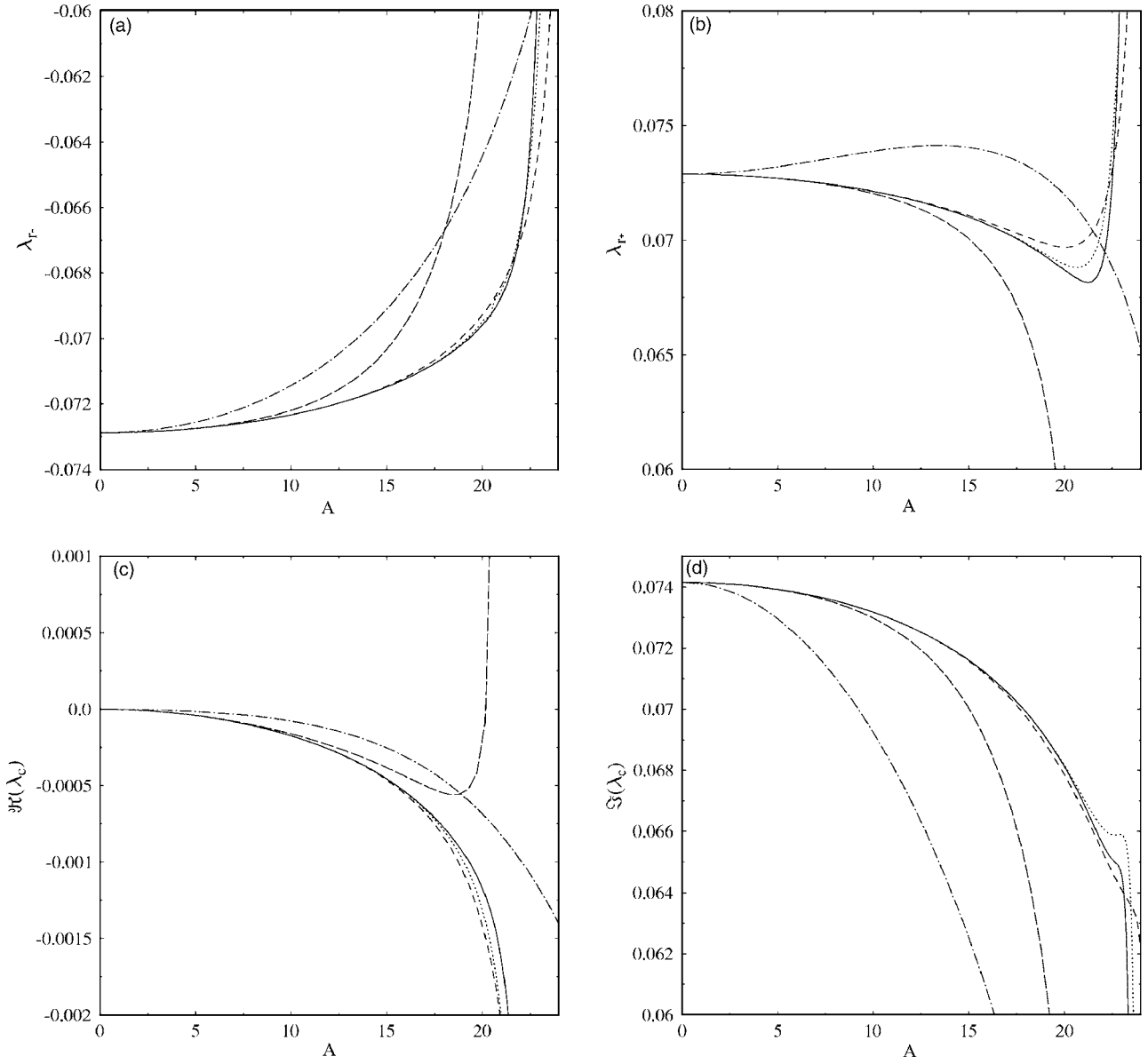

FIG. 9. The quantities (a) λ_{r-}, (b) λ_{r+}, (c) $\Re(\lambda_c)$, and (d) $\Im(\lambda_c)$ related to eigenvalues (24) of the Föppl systems of order (dashed-dotted) $N=1$, (long dashed) $N=3$, (short dashed) $N=5$, (dotted) $N=10$, and (solid) $N=15$ as a function of the area A of the EFHM vortex region.

quantities, i.e., λ_{r+}, λ_{r-}, $\Re(\lambda_c)$, and $\Im(\lambda_c)$, on the area A of the vortex region for several representative truncation orders N. As was the case with the loci of the higher-order equilibria, the largest modifications of the eigenvalues correspond to EFHM flows in which the vortex region is large and significantly deformed due to interaction with the obstacle. We notice that the magnitude of the eigenvalue λ_{r-} [Fig. 9(a)] decreases with the area A for all the truncation orders shown, while the magnitude of the eigenvalue λ_{r+} [Fig. 9(b)] behaves differently for different truncation orders. In contrast to the classical Föppl system, the real part of the complex eigenvalue λ_c is nonzero; it becomes negative with the magnitude increasing with A for all the truncation orders shown except for $N=3$, in which case the real part of λ_c becomes positive. In fact, $N=3$ is the only truncation order in which we detected complex eigenvalues with positive real parts. This anomalous behavior, affecting also other eigenvalues corresponding to $N=3$ [Figs. 9(b)–9(d)], appears related to a different shape of the equilibrium locus for this truncation order (Fig. 6). Finally, in Fig. 9(d) we notice that the frequency of the oscillatory mode decreases with A for all the truncation orders shown.

We emphasize that the most important qualitative difference between the linear stability properties of the classical Föppl system and the higher-order systems is that in the latter case the oscillatory mode is not neutrally stable, but for all truncation orders except for $N=3$ is exponentially stable. This property, resulting from the structural instability of eigenvalues with zero real parts, plays an important role in regard to applications of higher-order Föppl systems as models for flow control.

VI. DISCUSSION

In this section we briefly discuss certain properties of the higher-order Föppl systems important from the practical

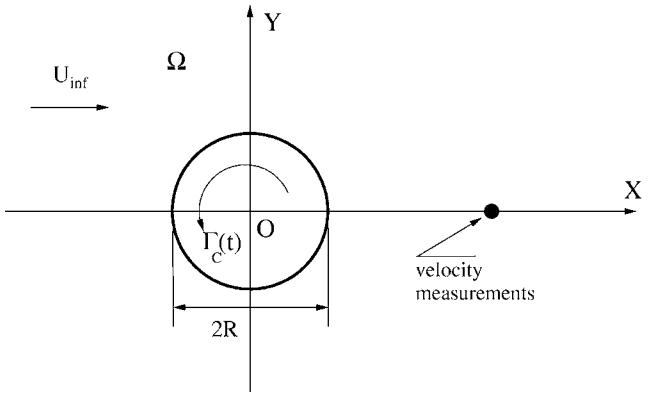

FIG. 10. Schematic of the wake stabilization problem.

point of view, especially, their utility as models for the design of feedback stabilization techniques for planar wake flows. In fact, the present investigation was motivated by our earlier work[8] in which a feedback wake stabilization algorithm was developed using the classical Föppl system as a reduced-order model. As summarized in Fig. 10, the problem consists in using the cylinder rotation, denoted Γ_C, as an actuation to prevent the onset of the vortex shedding instability with the system output in the form of velocity measurements on the flow centerline. Relevance of the classical Föppl system as a model of this phenomenon was established by Tang and Aubry.[25] An important control-theoretic limitation of the classical Föppl system is that with this particular actuation the oscillatory mode of the linearized system is in fact *not controllable*.[8] This means that the actuation (cylinder rotation) has no control authority over this mode. However, since the oscillatory mode is also neutrally stable, the linearization of the classical Föppl system is still *stabilizable*, even if it is not controllable. Nonetheless, this lack of controllability adversely affects performance of feedback stabilization strategies designed based on linearizations of the classical Föppl system and applied to more complex problems such as the control of the actual vortex shedding described by the 2D Navier-Stokes system. Furthermore, as recent investigations have shown, this uncontrollable and neutrally stable mode is related to the presence of a stable center manifold in the nonlinear Föppl system with feedback stabilization. As the results of Sec. V indicate, for all truncation orders except for $N=3$, the oscillatory modes present in the linearizations of the higher-order systems around the corresponding equilibria are in fact exponentially stable. This suggests that nonlinear higher-order Föppl systems can be easier to stabilize completely than the classical Föppl system when the cylinder rotation is used as the actuation. Preliminary results, reported in Ref. 28, concerning the design of control algorithms based on higher-order Föppl systems indicate that performance of such algorithms is indeed improved.

An important practical question is related to the choice of the parameters of a higher-order Föppl system when it is used as a model for control design for the Navier-Stokes system at a finite Reynolds number. This concerns both the choice of a specific Föppl equilibrium (3), as well as the choice of the area A of the EFHM vortex region and the truncation order N. With regard to the first choice, it was already encountered when designing controllers based on the classical Föppl system. A possible solution was outlined in Ref. 8, where it was proposed to choose the Föppl equilibrium (3) so as to obtain a desired length of the recirculation bubble. A similar approach could be adopted when a higher-order Föppl system is used, noting however that in addition to the circulation Γ_0 associated with the classical equilibrium (3), the recirculation length will now also depend on the area A of the vortex region (Fig. 3). With regard to the truncation order N, its choice should ensure sufficiently rapid convergence of the feedback-controlled state to the equilibrium and can be made based on numerical experimentation. Performance of feedback stabilization algorithms designed using different parameters characterizing a higher-order Föppl system is currently under investigation and results will be reported in the future.

Another family of reduced-order models commonly used in flow control problems is constructed using empirical eigenmodes obtained via the Proper Orthogonal Decomposition (POD).[29] The main conceptual difference with respect to the present approach is that the POD reduced-order models are derived from empirical data, such as time-dependent velocity fields, describing the system evolution, whereas the point-vortex models developed here are derived from the governing equations via suitable simplifications. Thus, these two families of reduced-order models represent two different approaches to the modelling problem and a comparison of their performance in flow control problems will be quite interesting. Recent results concerning feedback and open-loop control of vortex shedding using POD-based reduced-order models were reported in Refs. 30 and 31, respectively.

VII. CONCLUSIONS

In this investigation we constructed a two-parameter family of higher-order Föppl systems as generalizations of the classical point-vortex Föppl model.[1] The higher-order systems can be regarded as corrections of the classical (zero-order) system that approximate with adjustable accuracy the velocity field of steady Euler flows desingularizing the classical Föppl equilibrium.[4] The higher-order systems depend on two parameters: the truncation order N and the area A of the vortex region desingularizing the classical equilibrium. We studied the loci and the linear stability of the higher-order equilibria as functions of the two parameters. In particular, we found that with an increase of the area of the vortex region, the higher-order equilibria gradually move away from the classical equilibrium. Interestingly, the stability properties of the higher-order equilibria change and for all truncation orders except for $N=3$ the neutrally stable mode of the classical equilibrium becomes exponentially stable. We also argued that this finding may have important consequences for some problems in flow control, which had in fact motivated the present investigation. In this work we used the simplest nontrivial steady-state solution of the Euler equations available in the specific geometry of interest to us, namely the EFHM flow. As a matter of fact, analogous higher-order Föppl systems can be constructed using other,

more complicated, solutions of the Euler equations resulting in models possessing still more flexibility. Alternatively, potentially interesting point-vortex models of steady wake flows could be constructed using a larger, possibly infinite, number of vortices (e.g., a semi-infinite array). In addition, from the practical point of view, it would also be desirable to develop similar point-vortex models for other flow configurations of interest such as, for instance, flows past airfoils or backward-facing steps. This is, however, contingent on the possibility of finding suitable families of steady Euler solutions with constant vorticity vortex patches in these geometries. Such exercises are left for the future.

In view of the recent progress concerning computation of steady-state solutions of the Euler equations (see the review by Crowdy[11]), there appears to be another possibility to construct higher-order Föppl systems, namely, using the quadrature domain methods. As is well known,[19] every smooth compact planar domain, such as a detached EFHM vortex region, can be approximated by a sequence of quadrature domains with boundaries given by algebraic curves of increasing order. Since an algebraic curve has only a finite number of nonvanishing moments (9), it might be possible to construct an equation of the type (11) for every member of this approximating sequence. Another interesting question concerns construction of equilibria of an augmented system in which a number of moments of vorticity is used as dynamic variables in the spirit of the original investigation by Melander, Zabusky, and Styczek.[13,14] Investigation of such approaches and their relation to the present method is an interesting future research direction.

ACKNOWLEDGMENTS

The author wishes to express his thanks to Professor Alan Elcrat and Professor Ken Miller for many interesting and helpful discussions and for providing him with a code to reproduce the results of Ref. 4. This research was supported by NSERC (Canada) Discovery Grant.

APPENDIX: PROOF OF THEOREM 2

Here we present a sketch of a proof[32] of Theorem 2. By continuity, the limit of each intersection point of $C_n(x,y)$ and $D_n(x,y)$ is an intersection point of $C(x,y)$ and $D(x,y)$. By the Bézout theorem, there are the same numbers of intersection points (counted by multiplicities) of $C_n(x,y)$ and $D_n(x,y)$ independent of n and it is the same for $C(x,y)$ and $D(x,y)$. Therefore they must converge according to the multiplicities of the limits. □

[1] L. Föppl, "Wirbelbewegung hinter einem Kreiscylinder," Sitzb. d. k. Bayer. Akad. d. Wiss. **1**, 1 (1913).
[2] K. G. Miller, "Stationary corner vortex configurations," ZAMP **47**, 39 (1996).
[3] C. Marchioro and M. Pulvirenti, *Mathematical Theory of Incompressible Nonviscous Fluids* (Springer, New York, 1994).
[4] A. Elcrat, B. Fornberg, M. Horn, and K. Miller, "Some steady vortex flows past a circular cylinder," J. Fluid Mech. **409**, 13 (2000).
[5] G. Batchelor, "Steady laminar flow with closed streamlines at large Reynolds number," J. Fluid Mech. **1**, 177 (1957).
[6] G. Batchelor, "A proposal concerning laminar wake behind bluff bodies at large Reynolds numbers," J. Fluid Mech. **1**, 388 (1957).
[7] T. R. Bewley, "Flow control: new challenges for a new renaissance," Prog. Aerosp. Sci. **37**, 21 (2001).
[8] B. Protas, "Linear feedback stabilization of laminar vortex shedding based on a point vortex model," Phys. Fluids **16**, 4473 (2004).
[9] P. G. Saffman, *Vortex Dynamics* (Cambridge University Press, Cambridge, 1992).
[10] P. K. Newton, *The N-Vortex Problem, Analytical Techniques* (Springer, New York, 2001).
[11] D. G. Crowdy, "Quadrature domains and fluid dynamics," in *Quadrature Domains and Applications: The Harold S. Shapiro Anniversary Volume*, edited by P. Ebenfelt (Birkhauser, Boston, 2005), pp. 113–129.
[12] E. R. Johnson and N. R. McDonald, "The motion of a vortex near two circular cylinders," Proc. R. Soc. London, Ser. A **460**, 939 (2004).
[13] M. V. Melander, N. J. Zabusky, and A. M. Styczek, "Elliptically desingularized vortex model for two-dimensional Euler equations," Phys. Rev. Lett. **53**, 1222 (1984).
[14] M. V. Melander, N. J. Zabusky, and A. M. Styczek, "A moment model for vortex interactions of two-dimensional Euler equations. Part 1. Computational validation of a Hamiltonian elliptical representation," J. Fluid Mech. **167**, 95 (1986).
[15] L. M. Milne-Thompson, *Theoretical Hydrodynamics* (MacMillan, London, 1955).
[16] B. Fornberg, "Steady viscous flow past a circular cylinder up to Reynolds number 600," J. Comput. Phys. **61**, 297 (1985).
[17] N. E. Kochin, I. A. Kibel, and I. W. Rose, *Theoretical Hydrodynamics* (Ogiz, Leningrad, 1948) (in Russian).
[18] N. I. Akhiezer and M. G. Krein, *Some Questions in the Theory of Moments*, Transl. Math. Monographs Am. Math. Soc. (American Mathematical Society, Providence, 1990), Vol. 2.
[19] B. Gustafsson, Ch. He, P. Milanfar, and M. Putinar, "Reconstructing planar domains from their moments," Inverse Probl. **16**, 1053 (2000).
[20] J. L. Coolidge, *A Treatise on Algebraic Plane Curves* (Dover, New York, 1959).
[21] P. Henrici, *Applied and Computational Complex Analysis* (Wiley, New York, 1973).
[22] A. C. Smith, "On the stability of Föppl vortices," ASME J. Appl. Mech. **70**, 610 (1973).
[23] J. Cai, F. Liu, and S. Luo, "Stability of a vortex pair behind two-dimensional bodies," AIAA Paper No. 2001 (2001).
[24] T. W. G. de Laat and R. Coene, "Two-dimensional vortex motion in the cross-flow of a wing-body configuration," J. Fluid Mech. **305**, 93 (1995).
[25] S. Tang and N. Aubry, "On the symmetry breaking instability leading to vortex shedding," Phys. Fluids **9**, 2550 (1997).
[26] B. Sturmfels, *Solving Systems of Polynomial Equations* (American Mathematical Society, Providence, 2002).
[27] M. Marden, *The Geometry of the Zeros of a Polynomial in a Complex Variable* (American Mathematical Society, New York, 1949).
[28] B. Protas, "Vortex models for feedback stabilization of wake flows," in *Active Flow Control (Papers Contributed to the Conference "Active Flow Control 2006," Berlin, Germany, 27–29 September 2006)*, Notes on Numerical Fluid Mechanics and Multidisciplinary Design, edited by R. King (Springer, Berlin, in press).
[29] J. Lumley and P. Blossey, "Control of turbulence," Annu. Rev. Fluid Mech. **30**, 311 (1998).
[30] J. Gerhard, M. Pastoor, R. King, B. R. Noack, A. Dillmann, M. Morzyński, and G. Tadmor, "Model-based control of vortex shedding using low-dimensional Galerkin models," AIAA Paper No. 2003–4262 (2003).
[31] M. Bergmann, L. Cordier, and J.-P. Brancher, "Optimal rotary control of the cylinder wake using proper orthogonal decomposition reduced-order model," Phys. Fluids **17**, 097101 (2005).
[32] This proof was proposed anonymously at the discussion forum accessible through "Situs geometriae algebraicae," see archive available at http://www.math.washington. edu/sga